

Paleokarst features in the Aptian carbonates of the Barra Velha Formation, Santos Basin, Brazil

David Chibuzor Nworie^{1,2*} , Guilherme Furlan Chinelatto² , Alexandre Campana Vidal^{2,3} 

Abstract

Seismic data, borehole image logs, and conventional well logs were used to investigate the distribution and characteristics of paleokarst features in the Aptian carbonates of the Barra Velha Formation in a pilot area of the Santos Basin, Brazil. Multiple seismic attributes were used to enhance details on the seismic data and highlight key seismic parameters including strata deformation and geometry, continuity of seismic events, and fault patterns. The study found that karst structures are controlled by faults and fractures along structural highs, which served as a conduit for the flow of dynamic fluids that dissolved the carbonate materials. Several closed, circular depressions and bright spots identified in the northeastern portion of the study area represent possible sinkhole structures. Epigenic and hypogenic processes due to the action of meteoric water, hydrothermal activity, and intra-formation acidity along regional unconformities in the Barremian-Aptian may have been responsible for the dissolution. Limitations of this study are related to the difficulty of integrating multiple datasets with various scales. However, the higher confidence for the occurrence of the karst features is provided by borehole images at the sub-seismic scale. The findings of this study hold significant relevance for the strategic planning of energy development and carbon sequestration initiatives in the Brazilian continental margins, thereby aiding in informed decision-making.

KEYWORDS: Brazil; Santos Basin; pre-salt; Barra Velha Formation; carbonate reservoir; karst; fractures; seismic attribute analysis; image log.

INTRODUCTION

The term “Paleokarst” is commonly used to describe ancient dissolution features that develop due to chemical weathering processes, which may not be hydrologically connected to the current earth’s surface and have been preserved in the geological record (Wright and Smart 1994, Ford and Williams 2007, Aboaba and Liner 2020).

Paleokarst studies are an important aspect of carbonate petroleum reservoir evaluation due to its contributions to fluid flow (Zhang *et al.* 2021, Li *et al.* 2022). Diagenetic features such as dissolution structures and fractures influence the reservoir quality, and the understanding of their distribution could be useful in determining permeability anisotropies, preferred flow directions, or possible compartmentalization due to impermeable barriers (Watkins *et al.* 2018, Tanaka *et al.* 2022). Several studies have linked different karst development to the gradual and progressive enlargement of conductive fractures and faults which facilitate the flow of surface and deep-source

fluids (Kacaroglu 1999, Diabat *et al.* 2015). This dissolution in the carbonate reservoirs controls the size of pores, which may vary from small micro-scale cracks to meter-scale cave features (Xiaoxia *et al.* 2021).

Karst development has been attributed to near-surface karstification processes induced by multiple hydrogeological-related actions, which are eventually buried and subjected to further diagenesis (referred to as “epigenic” karst). On the contrary, “hypogenic” karst results from the action of acidic water and deep hydrothermal fluids in the subsurface (Milad and Slatt 2017). Hypogene karst can also be due to acidity developed within the rock (intrastratal or hypergene hypogene karst) because of the production of sulfide minerals without any connection to the surface or input of meteoric water. Intrastratal hypogene karst can be formed when sulfuric acid is generated within the rock due to the microbial activity or the oxidation of sulfide minerals. The acid dissolves the rock, creating voids that can eventually lead to the formation of caves and other karst features (Klimchouk 2013).

Distinguishing which process is prevalent has been a subject of discussion. However, the combined results of near-surface and deep-sourced processes may have resulted in observed spatial heterogeneities in various carbonate systems.

In the Santos Basin, Brazil (Fig. 1), the pre-salt succession is highly prospective due to the presence of a proven petroleum system (Beasley *et al.* 2010, Jesus *et al.* 2019). However, understanding the pre-salt prospects is challenging due to both poor seismic resolutions associated with imaging salt structures and the nearest underlying lithologies (Rodriguez *et al.* 2017) and the geological heterogeneities of the carbonate reservoirs

¹Department of Petroleum Science and Engineering, Universidade Estadual de Campinas – Campinas (SP), Brazil. E-mail: chibuzordavid3@gmail.com

²Centre for Petroleum Studies, Universidade Estadual de Campinas – Campinas (SP), Brazil. E-mails: gfcinelatto@gmail.com, vidal@unicamp.br

³Institute of Geosciences, Universidade Estadual de Campinas – Campinas (SP), Brazil.

*Corresponding author.



(Wang *et al.* 2015, Wright and Barnett 2015, Basso *et al.* 2020). Recent studies of the Brazilian Atlantic margin have reported on the lacustrine carbonates in the pre-salt succession (Okubo *et al.* 2015, Ribeiro da Silva and Pereira 2017, Rodriguez *et al.* 2017, Vincentelli *et al.* 2017, Wright and Barnett 2017a, Farias *et al.* 2019, Jesus *et al.* 2019, Basso *et al.* 2020, Chinellato *et al.* 2020, Gomes *et al.* 2020, Leite *et al.* 2020). However, there have been limited studies of the paleokarst structures in the pre-salt carbonates in the Santos Basin and their control on productivity, unlike other areas of the world such as in the Arkoma Basin, Tarim Basin, Campos Basin, where similar systems are relatively well known (Trice 2005, Xu *et al.* 2016, Basso *et al.* 2018).

A key problem for characterizing the Brazilian pre-salt carbonate reservoir especially as it relates to forecasting and optimizing production relates to the predictions of the non-matrix-based permeabilities and has become a crucial subject of research (Wang *et al.* 2015, Tanaka *et al.* 2022). In the pre-salt, karst and fractured zones have been seen to positively influence production due to excess permeabilities associated with its occurrence (Jesus *et al.* 2019). However, there is a need for careful considerations when dealing with these karst and fracture zones, as they may pose significant hazards to well development in situations of loss of mud, risking failure of well completions which could lead to serious complications or even total loss of the assets. Besides drilling complications, karst and fracture zones typically called thief zones are difficult to map on seismic due to their sub-seismic scale in most situations and issues associated with their capture on NMR measurements (Kumar *et al.* 2012, Mahry *et al.* 2016, Sallee *et al.* 2019, Maksimov *et al.* 2021).

Several prominent unconformities have also been identified within the rift and sag deposits of the pre-salt succession in the Santos Basin (Fig. 2) (Moreira *et al.* 2007, Leite *et al.* 2020). These unconformities occurred during periods of non-deposition and intense sub-aerial weathering dominated by dissolution and chemical alteration processes that resulted in the development of karst features, present in the pre-salt carbonate play in the offshore basins of Brazil (Bruhn *et al.* 2017, Basso *et al.* 2018).

Several methods have been used to investigate karstic features in seismic data by defining and predicting geometrical and

quantitative relationships between dissolution features and conduits such as fractures and fault networks (Klimchouk *et al.* 2016, Boersma *et al.* 2019). These methods are important processes for seismic evaluations of fractured/karstified carbonates and reservoir characterization, especially in the absence of close outcrop equivalent or sufficient core data for the Barra Velha Formation. Some popular filters and seismic attributes are as follows: the use of amplitude anomalies to identify caves (Basso *et al.* 2018) and the use of amplitude-sensitive attributes that were effective in highlighting bright spots and amplitude contrasts (Yu *et al.* 2016).

In addition, the use of coherence attributes to highlight faults and fractures associated with karst was adopted by Story *et al.* (2000), Basso *et al.* (2018), and Aboaba and Liner (2020). Similarly, Zeng *et al.* (2011) discussed the occurrence of circular fault structures related to collapse sinkholes highlighted using similarity attributes. Semblance and variance attributes have been used to delineate drainage patterns associated with paleokarst highlighted in regions of chaotic seismic expressions (Vahrenkamp *et al.* 2004, Chung *et al.* 2011), as well as subtle sinkhole features in the limestones in South Oklahoma (Aboaba and Liner 2020). Other methods include the use of structural filtering (Russel-Houston and Gray 2014), curvature and dip-related attributes (Sullivan *et al.* 2006, Qi *et al.* 2014), acoustic impedance inversion (Vahrenkamp *et al.* 2004), spectral decomposition (Ahlborn *et al.* 2014, Qi *et al.* 2014), and rock physics models (Sun *et al.* 2016).

Liu and Wang (2017) used a dip-steered coherence algorithm to help recognize faults and fractures associated with dissolution and dolomitization in a paleozoic carbonate reservoir in the Tarim Basin, NW China. Aboaba and Liner (2020) described the occurrence of vertical pipe structures related to sinkholes in a carbonate formation in the Arkoma Basin of Oklahoma using structural-based attributes. In the post-salt carbonates of the Macae Formation in the Campos Basin, Brazil, Basso *et al.* (2018) utilized seismic multi-attribute analysis classified by an unsupervised neural network to identify karstic features. Purdy and Waltham (1999) and Yao *et al.* (2005) used seismic equation-based diffraction models to identify karst features from host rocks.

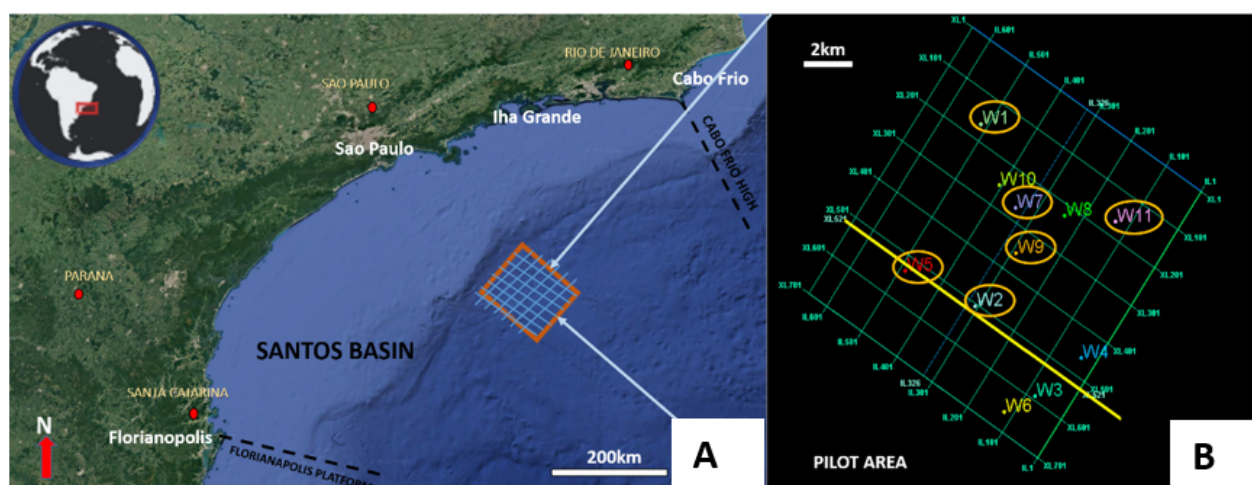


Figure 1. (A) Geographical location of the Santos Basin, in the SE Brazilian continental margin, bordered on the north by the Cabo Frio High and the Florianopolis High on the South. The study area is located on the outer high identified by the red box. (B) The distribution of the wells is displayed with the seismic grid of the pilot area.

In view of the limited studies on the paleokarst systems in the pre-salt succession of the Santos Basin, Brazil, this paper aims to present the findings on the characterization of the possible karstified and fractured regions in a pilot area (Fig. 1) in the Santos Basin, using multiple seismic attribute analysis that helped in highlighting structural features in the Barra Velha carbonate rocks. The relationships between karstification and structural features like fractures/faults as well as the driving mechanism for the dissolution in the study area were discussed using structure maps, pre-selected seismic volumes of amplitude, chaos, frequency, semblance, and sweetness attributes, as well as conventional well data and image logs analysis, which provided a greater resolution for observing these structures.

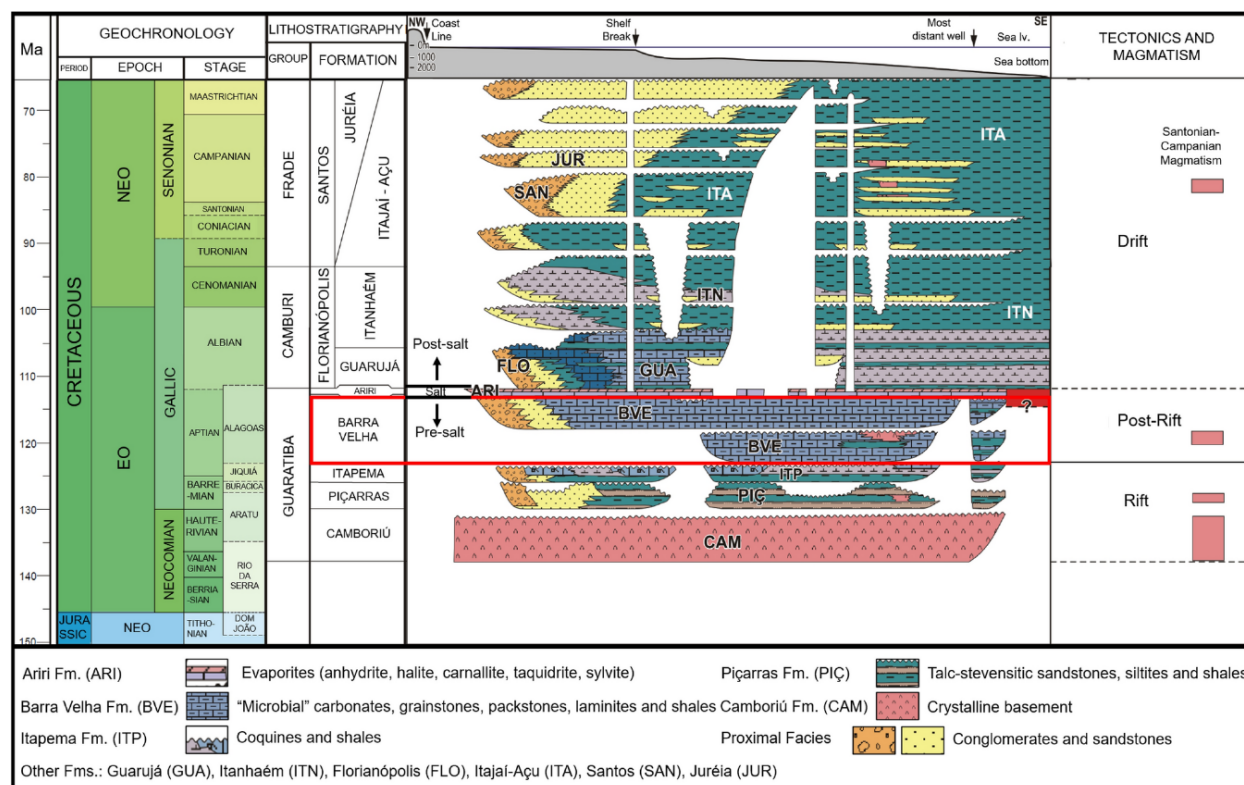
GEOLOGICAL SETTING

The Santos Basin (Fig. 1) is limited on the north by the Cabo Frio High that separates it from the Campos Basin, on the South by the Florianópolis High just before the Pelotas Basin (Ribeiro da Silva and Pereira 2017). The tectono-sedimentary evolution of the Santos Basin as discussed by Moreira *et al.* (2007) identifies six major unconformities within the Pre-salt sequence. The first two sets correspond to the top and base of the basaltic Camboriu Formation. The next unconformity called the Pre-Jiquia unconformity (PJU) limits the Picarras Formation. The PJU is overlain by the Itapema formation whose top is defined by the Pre-Alagoas unconformity (PAU). The Barra Velha Formation is divided into two depositional episodes by the Intra-Alagoas unconformity and separated from the overlying evaporitic Ariri formation by an unconformity

that signifies the end of the Rift/Sag phase of the basin evolution (Moreira *et al.* 2007).

The pre-salt succession is believed to be formed by the rift and sag phases (Ribeiro da Silva and Pereira 2017, Leite *et al.* 2020). During the rift phase, the sedimentary fill that lies unconformably on the Precambrian basement complex rocks made up of mixed suites of granites (igneous) and metamorphic rocks (Mizusaki *et al.* 1992) was deposited. Other sequences deposited in the rift stage include Picarras and Itapema Formation (Fig. 2) limited by the PJU and PAU unconformities, respectively. Gomes *et al.* (2020) reported that the Picarras and Itapema Formation are composed of talc-stevensite ooids that are interbedded with lacustrine coquinas and occasional organic-rich shales.

The post-rift super-sequence consists of lacustrine carbonates of Barra Velha Formation that underlies the Evaporitic Ariri Formation (Moreira *et al.* 2007, Ceraldi and Green 2016). Wright and Barnett (2017b) recognized three distinct facies in the Barra Velha Formation as follows: the calcite shub cementstones, calcite spherulite floatstones, and the Laminated calcimudstones. The shrubs consist of radiating fibrous calcites framestones encrusted in some cases with Mg silicates or patchy traces of former Mg silicates (Wright and Barnett 2017b), while the spherulites consist of calcite floatstones with silicate gels. The shrubs and spherulites are reworked into a new group of facies with varying textures influenced by intense weathering, which resulted in the fracturing and karstification identified in the carbonates of the pre-salt succession (Boersma *et al.* 2019). The coarsest reworked facies consist of well-sorted grainstones and/or packstones, which can have excellent reservoir quality (Wright and Barnett 2017a, Gomes *et al.* 2020). Finally, the drift



Source: adapted after Moreira *et al.* (2007).

Figure 2. Tectono-stratigraphic column of Santos Basin during the rift/sag phase. The Barra Velha Formation is highlighted by the blue box. The Barra Velha Formation in this session is emphasized with a red box.

phase believed to have been deposited from the Albian recently represents marine and non-marine sedimentation that is related to regressive and transgressive events (Moreira *et al.* 2007).

MATERIALS AND METHODS

Integrated seismic interpretation

The studied pilot session (Fig. 1) of the 3D seismic data covers an area of 300 km² covering the mound of an extensive carbonate reservoir in the Santos Basin. The vertical seismic resolution within these units is estimated to be 55 m with a sampling of 1,376 samples per trace. The seismic was processed with a standard reference of 0 m with a replacement velocity of 1,480 m/s. 3D Seismic profiles are displayed with SEG normal polarity, where an increase in acoustic impedance is represented by a positive reflection event (black), and a decrease in acoustic impedance is represented by a negative reflection event (red). Post-stacked 3D seismic data in depth were used to map the structures and horizons assisted by 11 wells (Fig. 1) widely distributed through the study area consisting conventional well logs (i.e., GR, Dt, RHOB, and Resistivity) and borehole images (BMI) that were used to define the stratigraphic correlation.

The top of the Barra Velha was mapped alongside three multilayered horizons based on the sonic and density log divisions that categorized the formation into three distinct zones. Depth slices were also studied on several intervals to identify structures and trends. Depth structure maps were generated for the interpreted horizons that were used in computing seismic attributes for the various levels of interest.

Seismic attribute evaluation

In this study, the identification of the changes of amplitude, phase, frequency, dip, continuity, and reflector configuration (geometry) was explored in order to identify regions of

relatively high fracture and karst probability. These signatures were then confirmed on the actual seismic section.

Amplitude attributes focused on applying seismic amplitudes in enhancing subtle details were used in identifying patterns and anomalies in the seismic data. Root-mean-square (RMS) amplitude was calculated by finding the square root of the amplitudes in a predefined window divided by the number of samples (Shelf 2002). Sweetness was derived by dividing the instantaneous amplitude by the root of the instantaneous frequency (Radovich and Oliveros 1998). This attribute may be useful in identifying lateral variability in rock units (Radovich and Oliveros 1998, Brown 2001). Anomalous amplitude events are often associated with changes in lithology or rock properties and allowed for delineating possible karst-related features. The geometry of these amplitude contrasts or anomalies were key in predicting the possible karst feature observed in the seismic data (Loucks 1999, Zeng *et al.* 2011, Basso *et al.* 2018).

Geometric seismic attributes extracted from the 3D seismic reflection data were useful in highlighting the geological features such as faults, stratigraphy, channels, and rock properties from seismic data (Chopra and Marfurt 2007). Edge detection, chaos, and similarity attributes were used to emphasize the regions of greater spatial amplitude variability and can indicate the areas of greater fracturing probability and highlight the zones of vug development and karstification (Oliveira *et al.* 2019). These attributes consider the lateral amplitude variation along the structural dip and result in a small-scale discontinuity (high frequency) volume.

The frequency-based attributes were calculated by filtering the seismic data at various frequency ranges (16–52 Hz) to show certain geological patterns that may not be obvious in the other frequency bands. The separation and classification of the seismic events based on their frequency content were facilitated by the spectrogram and power spectrum (Fig. 3). The power spectrum and spectrogram (Fig. 3) were created

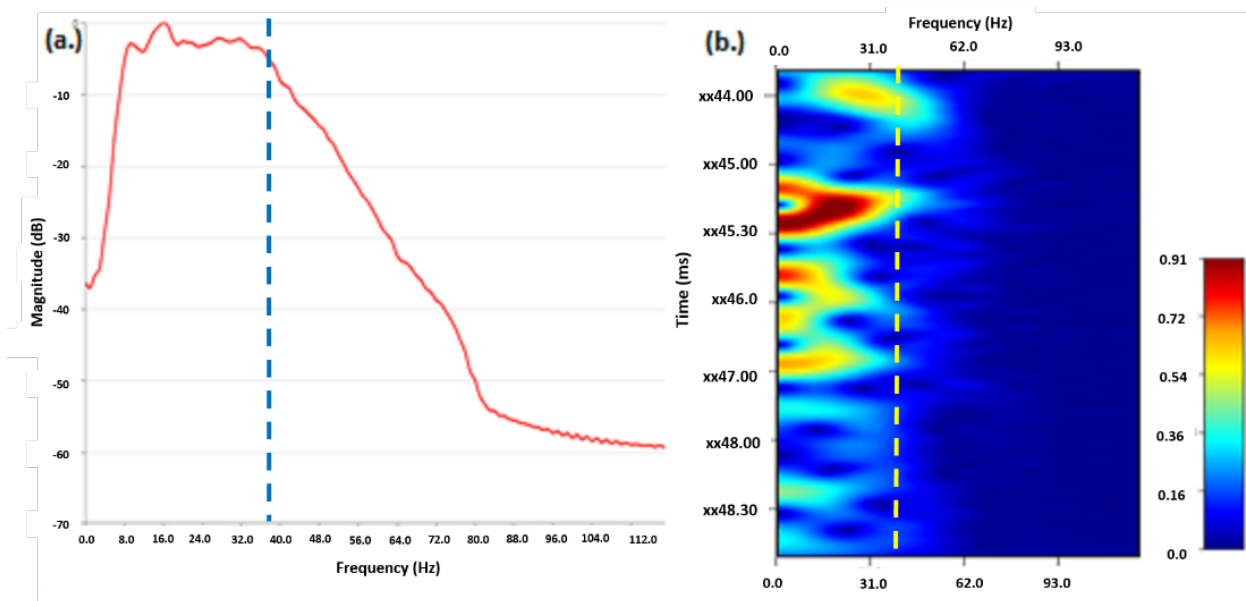


Figure 3. (A) Power spectrum showing the dominant frequencies across the spectrum. (B) Spectrogram showing the dominant frequency with time. A frequency of 40 Hz was selected as optimum for the spectrum shown in the blue line on the power spectrum and in the yellow line on the spectrogram.

and analyzed to determine the dominant frequencies and trend with respect to time. A frequency of 40 Hz was found to be most optimal in capturing the dominant seismic signals.

Acoustic borehole image

For this work, a total of six wells (circled in Fig. 1) with acoustic borehole images were evaluated and used to describe karstic features with a resolution of 0.5 m. The image set was obtained from the Ultrasonic Borehole Imager (UBI, Schlumberger) and Circumferential Acoustic Scanning (CAST, Halliburton) tools, and an average of 290 m of the image from the Barra Velha Formation was described. Three types of images were used for descriptions, the static and dynamic amplitude images that show the main borehole wall characteristics (acoustic impedance of the borehole) and the travel time images that give the 360° borehole caliper which is useful for highlighting open fractures, breakouts, large vuggy pores, and caves.

The acoustic borehole images provide the acoustic impedance of the borehole wall where geological features such as sedimentary beddings, rock texture, faults, and fractures can be identified. From the analysis of static and dynamic images, a low acoustic impedance signal represented by dark-colored traces is generally interpreted to indicate non-mineralized features such as vugs, fractures, caves, and breakouts. The high acoustic impedance is represented by lighter-colored traces and interpreted as the rock matrix.

The travel time images provide the caliper of the borehole (borehole shape) and highlight some geological features such as large vugs, open fractures, channels, and caves as well as breakouts. In this image type, the void spaces are captured and enhanced in comparison with the rock matrix, but features such as bedding or rock texture are not represented. By combining all images, it was possible to justify and support some

geological interpretations such as the occurrence of vugs, open fractures, caves, and breakouts.

RESULTS

Integrated seismic interpretation

The carbonates of the Barra Velha Formation are overlain by the evaporites of the Ariri formation, which is characterized by a flat GR response. The top of the Barra Velha Formation is represented by nine peaks on the GR log regarded as a regional marker in the pre-salt succession (Wright and Barnett 2017a, Gomes *et al.* 2020). The Barra Velha Formation varies in thickness laterally across the wells from about 139 to 420 m with an average of 283.18 m. In general, the GR response along the Barra Velha Formation shows low readings with an average of 20.39 API, which is indicative of relatively clean carbonates with low radioactive constituents.

Four main horizons were mapped within the Barra Velha Formation based on the zonations defined from the resistivity and sonic-NPHI logs (Fig. 4). The mapped horizons include the top of the Barra Velha formation (BV Top), two intermediate horizons (BV 001 and BV 002), and the base (BV Base) (Fig. 5).

BVTop is characterized by bright continuous red reflection in the seismic data, due to the high acoustic impedance difference between the salt layer and the underlying carbonates. The boundary is distinctive due to the presence of the angular unconformity separating the two formations. BV 001 was mapped on a wavy thin black reflector that lies within the Barra Velha Formation. It occurs as a discontinuous surface with a few truncations that can be attributed to faults, dissolution/karstification, and seismic resolution. BV 002 is similar to BV 001; However, it is a black discontinuous wavy reflection

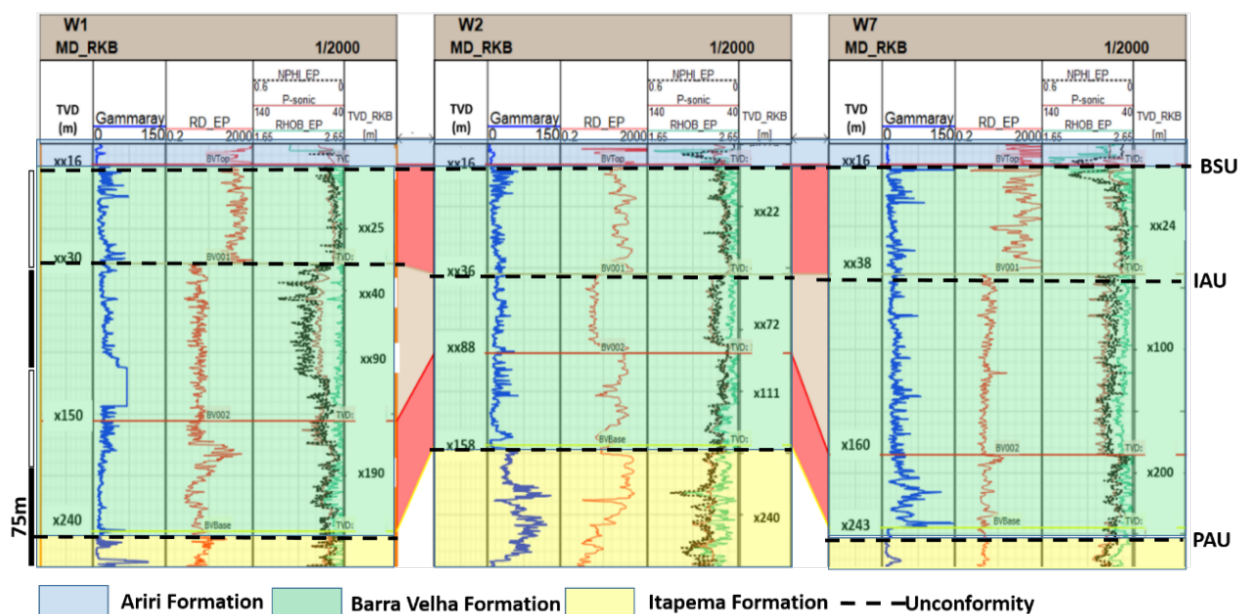


Figure 4. Correlation across three wells (W1, W2, and W7) in the study area showing the stratigraphic positions of the mapped horizons with emphasis on the Barra Velha Formation. BSU (BVTop) represents the base of the salt uniformity that is identifiable on seismic due to the angular unconformity between the Ariri Formation and the Barra Velha Formation. IAU (BV001) represents the Intra-Alagoas unconformity that separates the upper and lower Barra Velha Formations.

(Fig. 5). The base of the Barra Velha Formation (BV Base) is represented by a strong peak that corresponds to the Pre-Alagoas unconformity. Table 1 summarizes the characteristics of these horizons as explained above and shown in Fig. 5. The depth horizon maps (Fig. 6) show an undulating topography with limbs dipping away from each other in the W-E direction on the inlines and crosslines (Fig. 7).

The depth structure map of the Barra Velha formation (BV Top and BV Base) (Fig. 6) shows distinct regions of high relief (hot colors) and regions of low relief (cold colors). The seismic patterns common to the pre-salt sequence include divergent, parallel continuous, disrupted wavy, and chaotic patterns restricted to the lower sessions of the seismic (Table 2).

Fractures, faults, and paleokarsts from seismic attribute evaluation

The edge detection surface of the top of the Barra Velha Formation shows the relatively continuous regions in blue with the possible discontinuities in red (Fig. 8A). When compared with the maximum curvature surface (Fig. 8B), the major and minor fault lines in green were observed to be trending in the Northeast–Southwest direction. The curvature surface shows the change in dip and azimuth of the 3D seismic reflection surface (Roberts 2001), with the most positive zones in green indicative of faults (Sullivan *et al.* 2006). The highlighted discontinuities are pronounced in the eastern region of the study area with more fractures situated on the structural high surrounded by wells W8, W9, W11, and W4 (Fig. 8B).

The amplitude-based attribute surfaces (Fig. 9) show a series of bright spots that relate to zones of high impedance contrast between the host rock and possible karstified regions. In the Southwestern region, long patches of bright spots were spotted, and upon taking a cross section across

the structure in the north–south direction, elongated bright spots that correspond to a cluster of observed mini-faults with limited displacements were observed. The chaos section of this cross-section shows discontinuous zones in black (highlighted by red arrows in Fig. 9) extending from the top toward the base of the Barra Velha Formation. “Pearl structures” (“Beads of Bright Spots”) were also observed along these damage zones representative of possible collapse structures as observed by Tian *et al.* (2016) in the Ordovician Carbonates in the Tarim Basin.

Chaos and variance surfaces of the top of the Barra Velha Formation show the main fracture corridors (Figs. 10 and 11), located along and parallel to the major faults highlighted as dark-colored lineation. The cluster of possible fractures swam around the major faults and are seen to be more dominant on the structural highs. Circular depressions highlighted by red arrows (Figs. 10 and 11) are also feasible in the eastern portion, which may be attributed to the occurrence of possible sinkholes like those identified by Basso *et al.* (2018) and Aboaba and Liner (2020). Some possible erosional features are highlighted by the chaos and variance attributed toward this region occurring as dark lineation extending in the northeast-southwest direction. These erosional features and intense fracture occurrence are emphasized by the coblended surface of chaos, variance, and frequency shown in Figs. 11 and 12 localized on the structural high.

Clusters of fractures identified on the geometric attributes such as semblance correspond to bright spots identified on the RMS amplitude and sweetness volume (Figs. 13 and 14). The areas of high semblance are in white color, while low semblance areas are chaotic with grayish-dark coloration. The suspected fractures are visible in the low semblance regions as dark gray lines on the map view and dark gray discontinuities

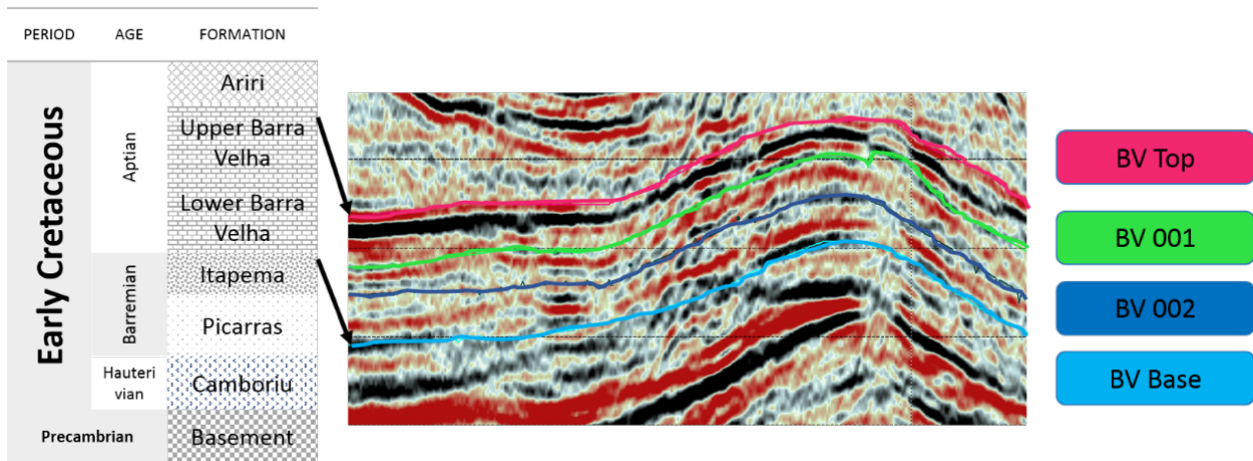


Figure 5. Mapped horizons on the seismic data, illustrating reflection patterns and age correlation in the study area. The top and base of the Barra Velha Formation are highlighted by the red and blue horizons, respectively.

Table 1. Characteristics of horizons mapped in the study area. The table summarizes the horizon name, characteristics, and reflector type.

SN	Horizon	Characteristics	Reflector
1	BV Top	Strong bright continuous reflection with overall divergent configuration	Tough
2	BV 001	Discontinuous black reflection	Peak
3	BV 002	Discontinuous red parallel reflection	Tough
4	BV Base	Discontinuous red reflection with strong reflections on some parts of the seismic	Tough

of the whitish high semblance regions on the crossline/inline. Crossline B (XLB) located entirely on the structural high shows the distribution of bright spots across the length of the section. However, crossline A (XLA) that cuts through a portion of the structural high and low shows the placement of the bright spots and possible fracture zones toward the eastern structural high (Fig. 13).

Karstic features from image log analysis

According to the images logs, four main karst-related features were described from six wells studied: (1) vuggy zones, (2) open and enlarged fractures, (3) caves, and (4) breccia derived from reworking of in-situ facies and brecciation along faults (Fig. 15). Vuggy zones and open and enlarged fractures are the most common features, whereas caves and breccia occur only in a few intervals in wells W1, W4, and W8. Vuggy pores correspond to dark-colored traces in both static and dynamic images. The open and enlarged fractures are represented by the occurrence of dark-colored irregular sinusoidal traces in all borehole images (Fig. 15B), and the aperture may vary according to the degree of dissolution.

The caves are relatively easy to identify in the acoustic borehole images, as they are represented by a dark-colored area extending vertically or horizontally which is distributed

due to the effects of dissolution based on structural or mineralogical controls (Fig. 15C) and are larger compared to open fractures or vugs. Lastly, the breccia is identified only in static and dynamic images, occurring as high acoustic impedance compared with the matrix that surrounds them (Fig. 15D).

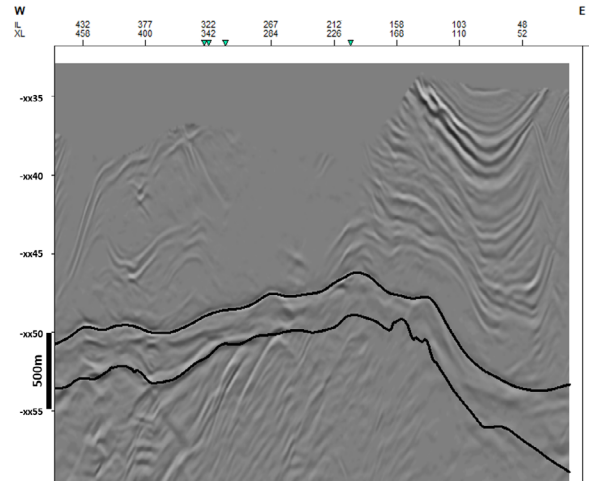


Figure 7. Cross section of the Barra Velha Formation along the red line in Fig. 6 showing the depth structure and internal reflections of the formation in grayscale. The top and base of the Barra Velha formation are highlighted by black lines.

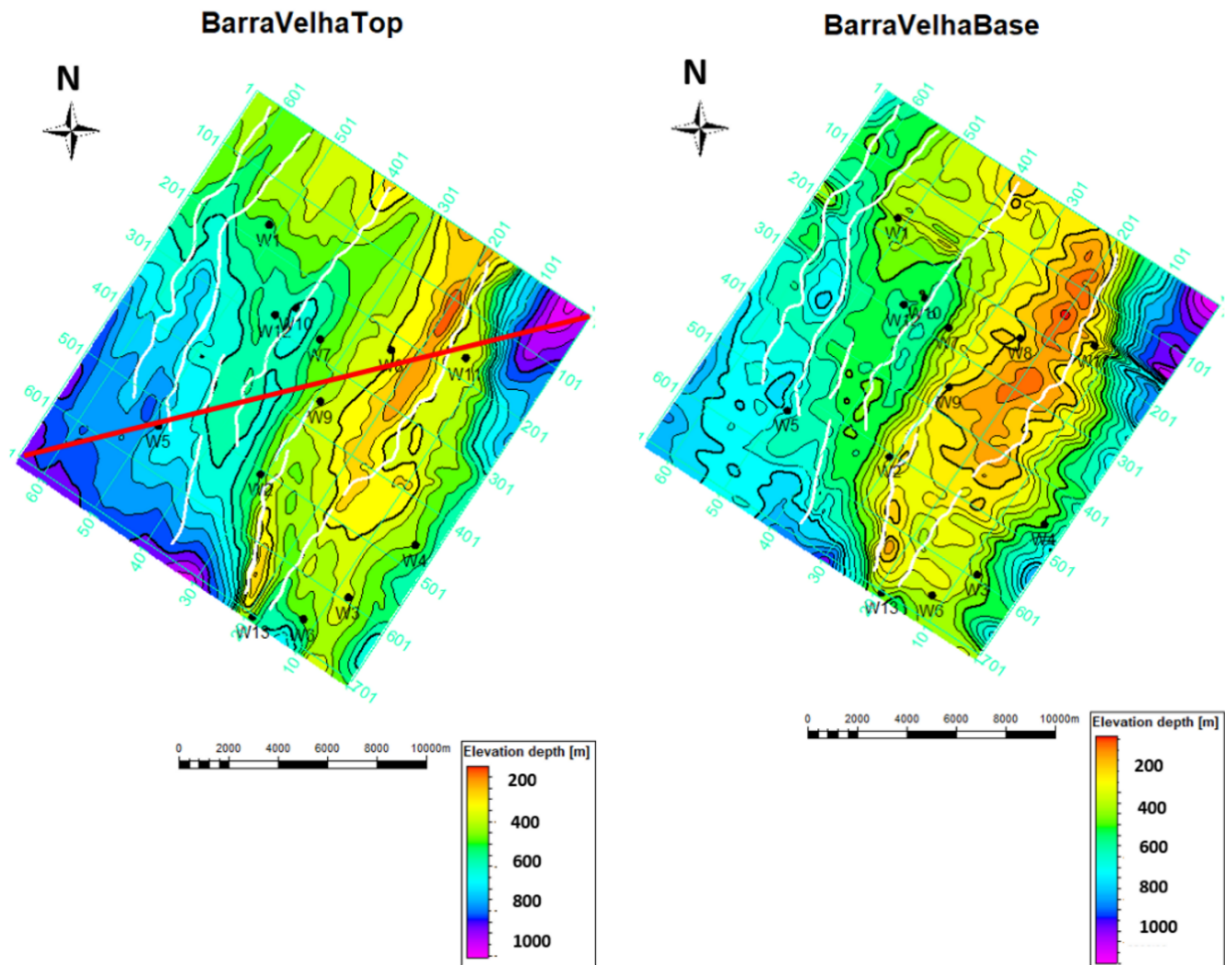


Figure 6. Depth structure map showing (A) top of the Barra Velha Formation (BV Top) and (B) base of the Barra Velha Formation (BV Base). Hot colors correspond to the structural highs, while cold colors represent the structural low domains. The red line represents the cross-section displayed in Fig. 7.

DISCUSSION

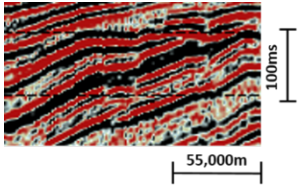
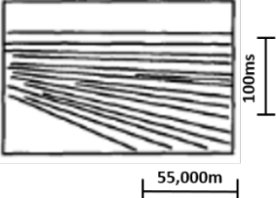
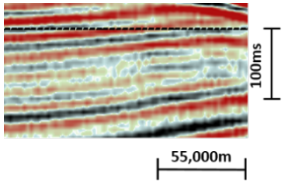
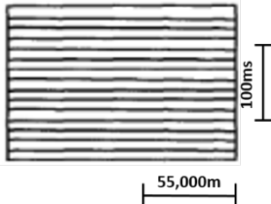
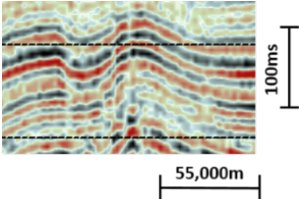
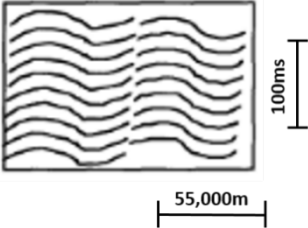
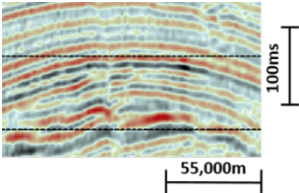
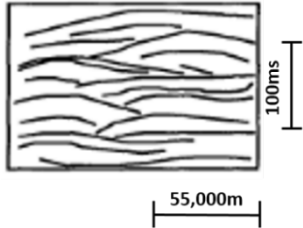
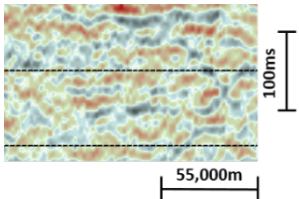
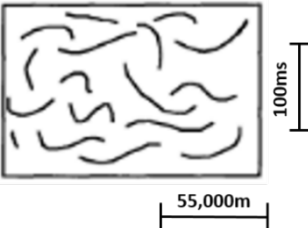
The complexity of paleokarst reservoirs makes seismic imaging and interpretation a challenging task. In an attempt to define the distribution of karstic features, many authors make use of seismic attributes combined with geological interpretations for its delineation (Purdy and Waltham 1999, Yao *et al.* 2005, Liu and Wang 2017, Basso *et al.* 2018, Aboaba and Liner 2020). In this study, multiple seismic attribute analyses alongside conventional well data and borehole images were used in characterizing the occurrence and distribution of paleokarst systems in the Aptian carbonates in the Barra Velha Formation of the Pre-salt succession in the Santos Basin, Brazil.

Possible paleokarst features in the study area are represented by high amplitude contrasts in the seismic data representing the difference between the properties of the host rock and the karstic feature which could either be void or filled

as pointed out in other oil fields around the world (Yu *et al.* 2016, Rodriguez *et al.* 2017, Basso *et al.* 2018, Aboaba and Liner 2020). The amplitude-based attributes were compared with other independent attributes to reduce the likelihood of obtaining spurious correlations.

According to the results of this study, faults and fractures may represent the main conduit systems for the dissolution of carbonates, with karst features tending to develop from the enlargement of these rock discontinuities within the Barra Velha Formation. The presence of faults can create pathways for the infiltration of water and the circulation of fluids, leading to enhanced dissolution and the formation of distinctive karst features. The enlargement of faults and fractures can be driven by a variety of factors, including the presence of weak layers, the migration of fluids, and the action of tectonic stresses. These factors can create zones of increased porosity and permeability

Table 2. Reflection configurations and seismic facies' descriptions.

Seismic facies Description	Example from the data	Reflection geometry	Interpretation
A <i>Tilted beds</i>		Divergent	
B <i>Planar bedded</i>		Parallel continuous	
C <i>Deformed/Wavy</i>		Parallel Disrupted/wavy	
D <i>Mound-shaped</i>		Mound-shaped/discontinuous	
E <i>Chaotic</i>		Chaotic	

Source: adapted after Laurent *et al.* (2021).

along the fault plane, which in turn promotes dissolution and the development of karst features.

The bright spots observed in association with fault and/or fracture zones may be linked to the development of sink-hole features located at the crest and roof of the cave or passage systems, as depicted in Figs. 14 and 16. Conversely, in regions where clear discontinuities are not readily apparent,

such as in Figs. 10 and 11, these bright spots may be related to the presence of paleo-drainage paths. Anomalous amplitudes and bright spots were also identified among chaotic seismic reflections with minor fault indications (Tang *et al.* 2021) which is similar to the Ordovician Carbonates in the Tarim Basin (Zeng *et al.* 2010). The presence of anomalous amplitudes and bright spots in regions with minor fault indications

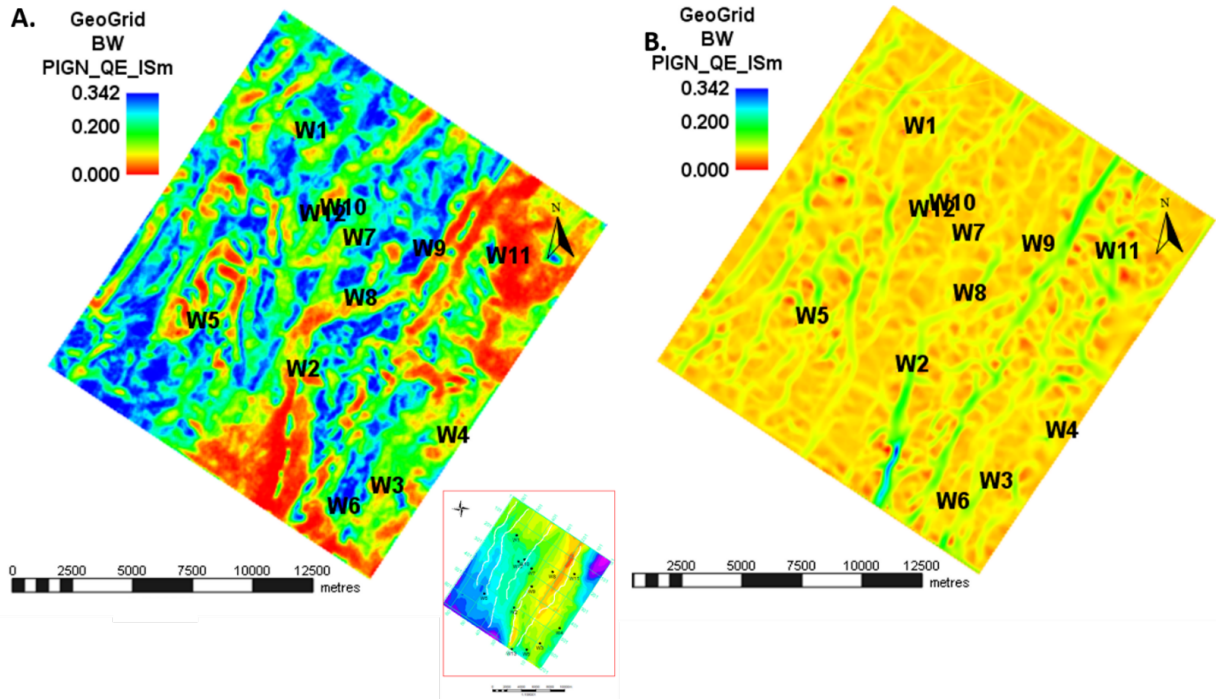


Figure 8. Seismic attribute maps of the Barra Velha Formation top. (A) Edge detection and (B) maximum curvature maps, highlighting amplitude contrast regions with red and green colors. These low-amplitude regions are parallel and directly related to the high fracture and fault zones in the study area. The edge detection map highlights the edges of the amplitude contrast regions, while the maximum curvature map indicates the curvature of the seismic wavefronts, with high curvature values indicating the presence of faults or/and fractures.

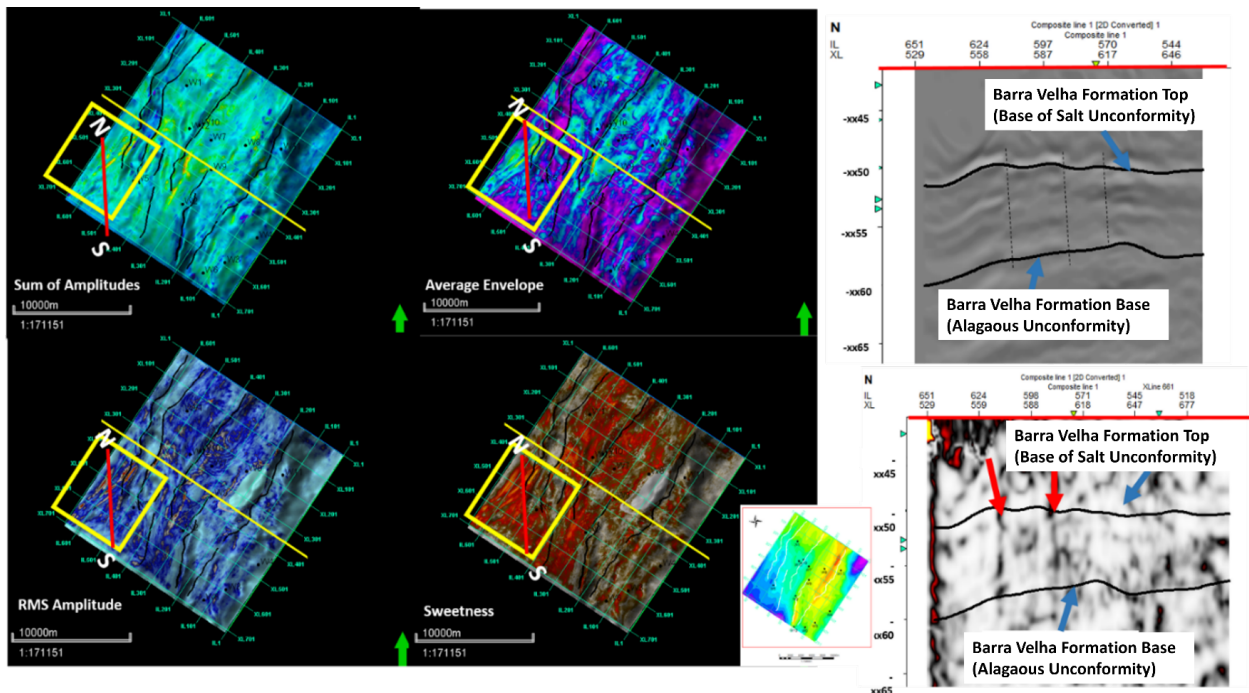


Figure 9. Amplitude-based seismic attribute surfaces (i.e., Sum of Amplitudes, Average Envelope, RMS Amplitude, and Sweetness) of BVF Top. The attribute surfaces display bright spots indicative of zones of high impedance contrast between the host rock and possible karstified regions as elongated patches visible in the southwestern region. The chaos section of the cross section across these anomalies (N-S) shows discontinuous zones in black (highlighted by red arrows, extending from the top toward the base of the Barra Velha Formation).

suggests that other geological features or processes may be driving the observed seismic anomalies.

The edge detection and maximum curvature attribute maps (Fig. 8) reveal the presence of widespread anomalous bright spots, associated with the fault and discontinuities on the top of Barra Velha Formation. Similarly, Sullivan *et al.* (2006) and Qi *et al.* (2014) in their study related this occurrence of discontinuity with positive values on the curvature surface with collapse features associated with a system of faults and joints, which is consistent with the results of this study. The low amplitudes identified on the amplitude-based attributes (Fig. 9) are believed to be associated with karstification, especially with the occurrence of bright spots and pearl structures (Ahlborn

et al. 2014, Li *et al.* 2016, Sun *et al.* 2016) or bead-like reflections (Sun *et al.* 2013, Basso *et al.* 2018).

No fluvial system was identified from the seismic or image log in this study. However, the chaos surface shows the occurrence of dark lineation, which is concentrated along the structural highs and around fault locations (Figs. 10A and 16). The dark lineations observed in the chaos surface may be attributed to the presence of intrastratal karst features, such as solution-enlarged fractures and bedding planes or to the effect of fluid flow along these preferential pathways. The association of these features with the structural highs and fault locations suggests that they may be related to the tectonic and structural history of the Barra Velha Formation. Further studies incorporating

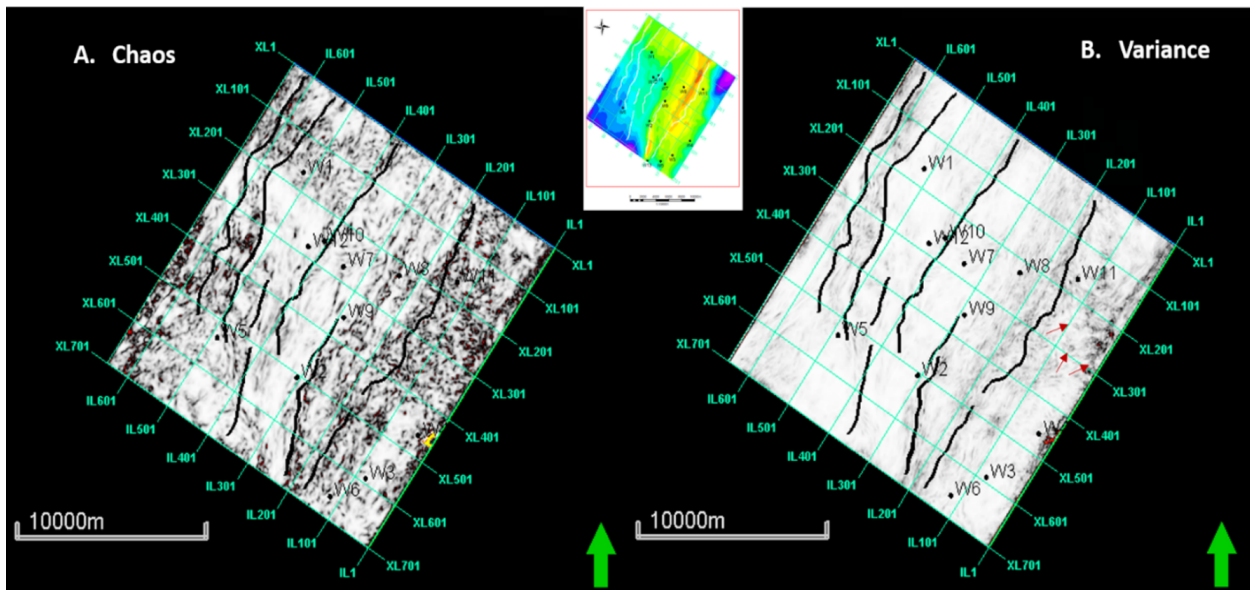


Figure 10. (A) Chaos surface showing faults in black lines. Possible fracture zones are seen with dark paths. (B) Variance map showing circular structures related to possible sinkholes in the Northeastern portion of the area. Low similarity corresponds to high amplitude region volumes. Low similarity (dark lineation) corresponds to high amplitude (hot colors) region highlighted with red lines.

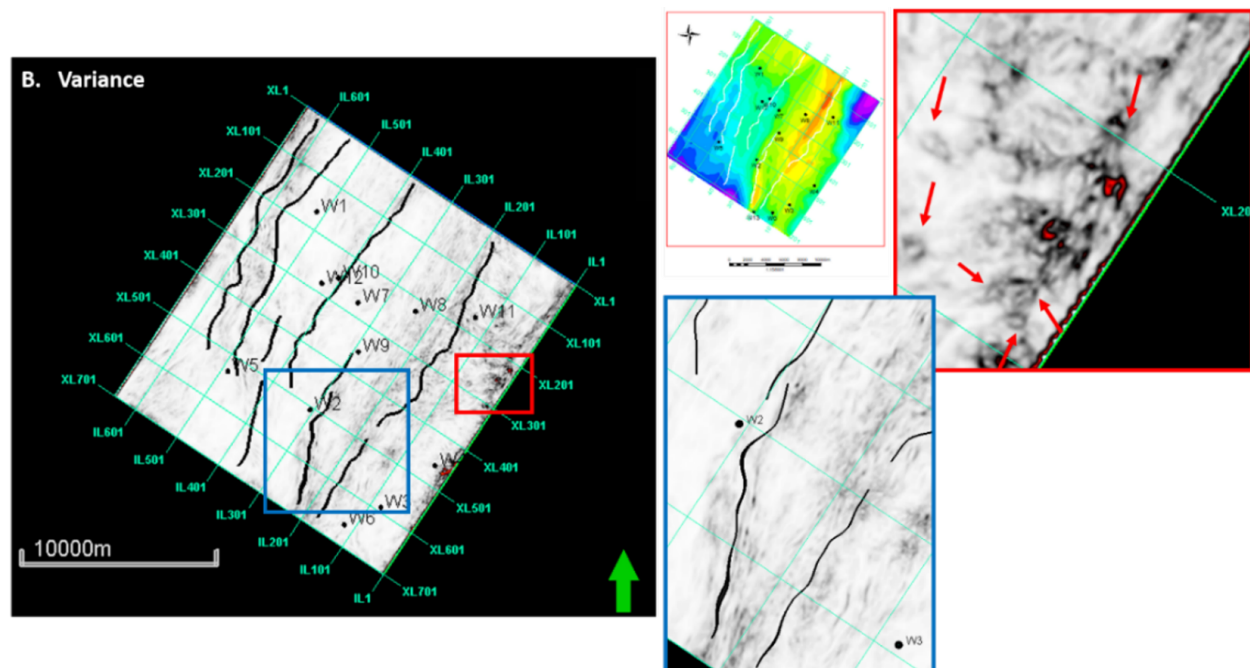


Figure 11. Zoomed-in view of the variance surface from Fig. 10, highlighting the possible sinkhole structures and high fracture intensity zones. The main fractured corridors are located along and parallel to the major faults and are dominant on the structural highs. Circular depressions, which may be attributed to possible sinkholes, are feasible in the eastern portion and are highlighted by red arrows.

additional data and methods, such as geochemical analysis and sedimentology, may provide additional insight into the depositional and landscape history of the Barra Velha Formation.

The variance surface (Fig. 10B) provides information on the dominant orientations of the possible fractures whose intensity seems to be influenced by the structural positions and location of faults (Figs. 11 and 12). Circular depressions, which may be indicative of sinkhole structures, were observed in the northeastern portion of the study area, as highlighted by the red arrows in Figs. 11 and 12. The occurrence of these

sinkhole structures may be attributed to the process of dissolution and collapse of the underlying carbonate rocks, which is a common feature of karst landscapes.

The discontinuities are widely distributed but tend to occur in higher intensity toward the breakpoints of the paleo-highs and are dominantly trending in the Northeastern–Southwestern direction. The fractures/faults generally trend in the Northeast–Southwest direction, which is the principal structural trend of the study area. There is also a correlation between the fractures/faults identified on the

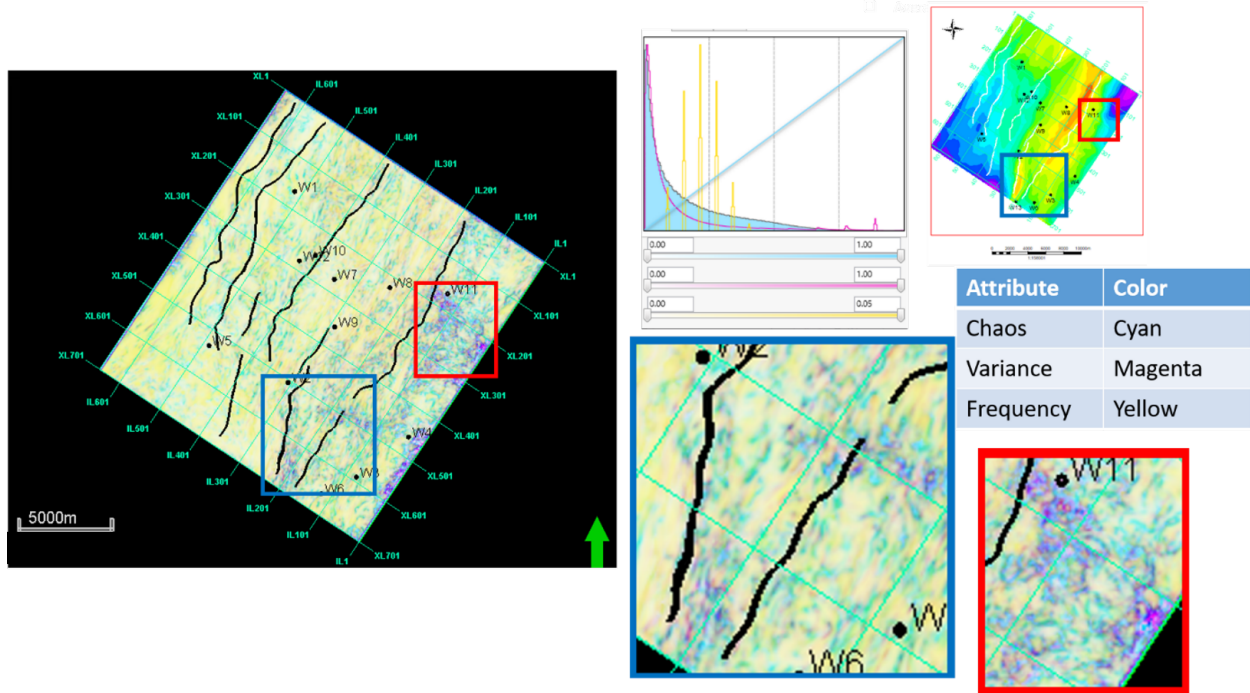


Figure 12. Coblended surface of chaos, variance, and frequency showing possible erosional zones and features displayed using CMY format. Fracture corridor and erosive feature are highlighted in blue and red boxes, respectively. The possible fracture and erosional features, occurring as lineation extending in the northeast–southwest direction, are emphasized on the structural high.

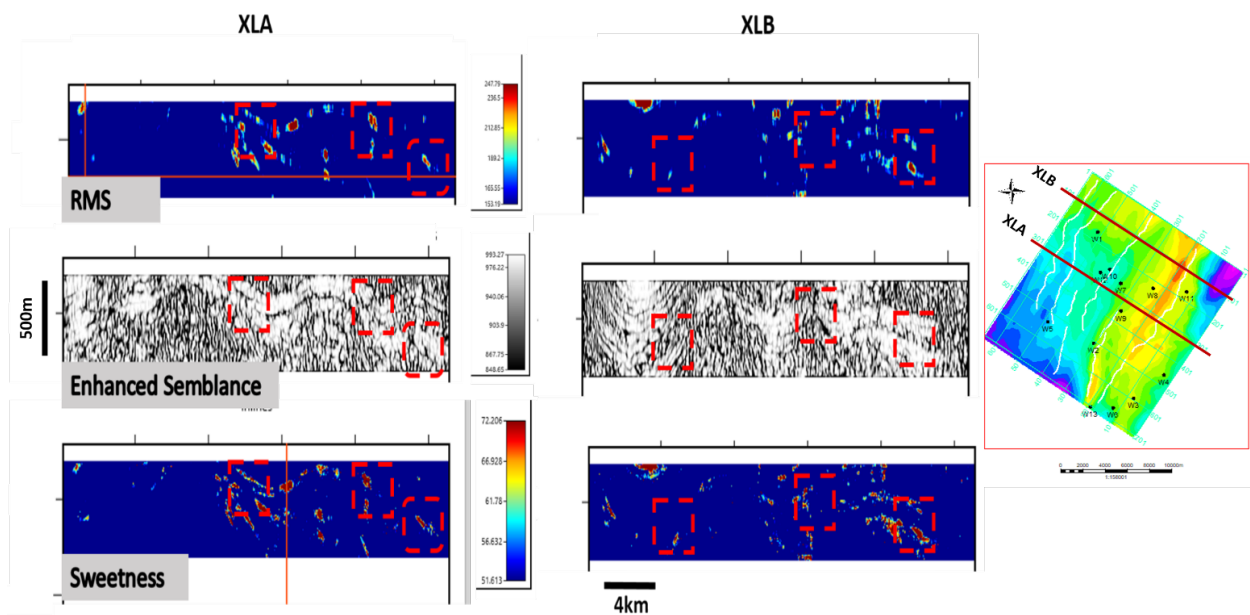


Figure 13. Semblance showing the correlation between the low semblance regions with high amplitudes from Sweetness and RMS volumes. Possible fracture zones are highlighted using red boxes. Structural map showing the position of the crosslines is displayed, with Crossline B (XLB) located on the structural high and Crossline A (XLA) cutting through a portion of the structural high and low. The areas of high semblance are in white color, while the low semblance areas are chaotic with grayish-dark coloration.

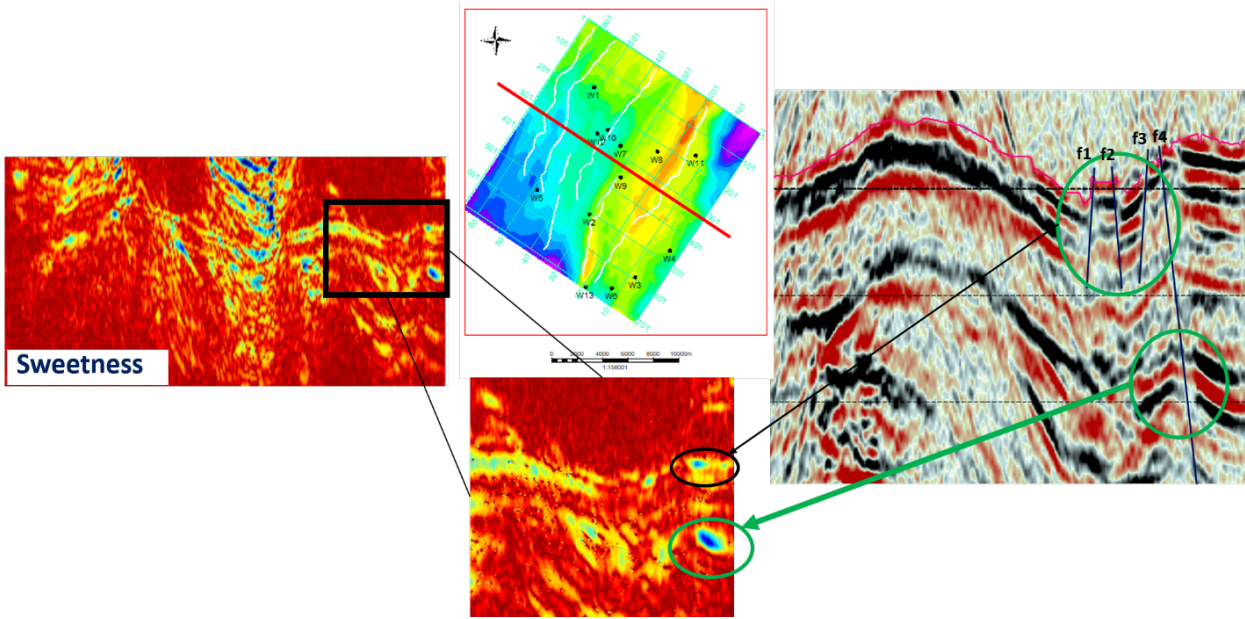


Figure 14. Sweetness attribute for Crossline 251. The green circles signify the anomalous amplitude that corresponds to the highly fractured region on the seismic. The horizons appear to be significantly collapsed across the levels with possible sinkhole occurrence. The horizons show a significant collapse across the levels, indicating possible sinkhole occurrence in the area.

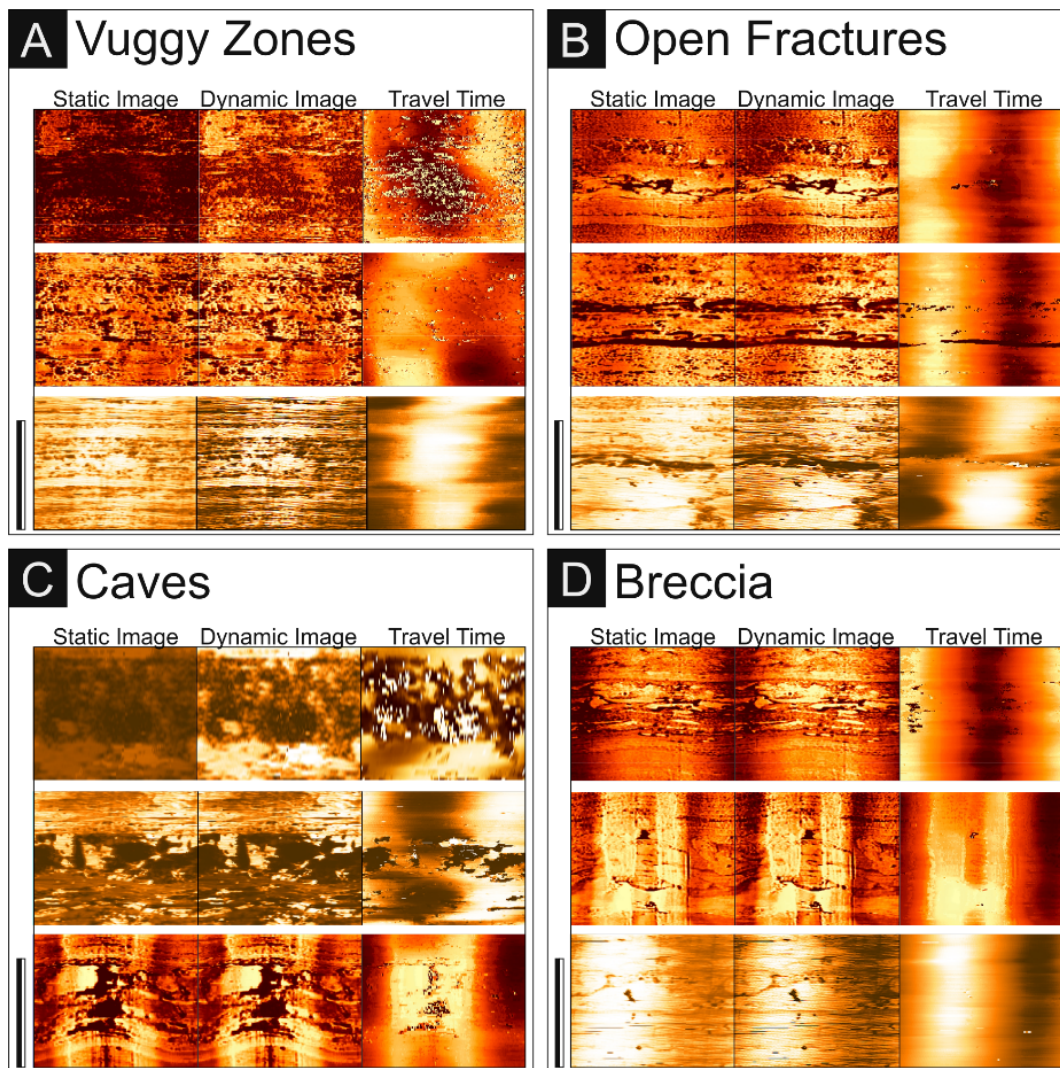


Figure 15. Examples of karstic features described in acoustic borehole image logs. Three types of images are illustrated: static, dynamic, and travel time. (A) The vuggy zones occur as dark traces in static and dynamic images and cold appear or do not in travel time images according to their size. (B) Occurrence of open fractures highlighted by the sinusoidal dark trace in all images. (C) The caves are much bigger compared with the vug pores and are observed in all image logs. (D) The breccia is observed only in static and dynamic images and is identified according to the variation of acoustic impedance between clasts and matrix. The scale bar in all examples corresponds to 1 m in a vertical orientation.

high semblance regions with high amplitude contrast regions on the RMS and sweetness volumes, which are common on the high relief areas highlighted in red boxes (Fig. 13). The paleohighs appear to have a high concentration of dissolution and erosion evident by the dominance of fractures indicated by similarity attributes and high amplitude contrast zones, with the paleolows with less occurrence of this phenomenon.

The average amplitude and RMS also highlight the relationship between the possible fractured zones and the high amplitude contrast regions (Figs. 9, 13, and 14). However, the high amplitude regions do not necessarily correspond to these fracture/faulted zones. An example of highlighted fractured/faulted zone is indicated by the yellow box (Fig. 9). These seismic amplitude contrasts are also associated with chaotic seismic reflection (Table 2) and faulted zones, regarded as structurally damaged zones that have been previously associated with karstification and intense fracturing by previous literature. These sorts of features are seen to enhance or destroy impedance contrasts within a stratigraphic architecture (Janson and Fomel 2011).

The suspected karst geometry in the Barra Velha Formation carbonate occurs as isolated circular or linear features (Fig. 11) which may be sinkholes or/and elongated patches closely associated with the fractured/faulted zones indicative of structurally damaged zones as described by Zeng *et al.* (2011) in the Tarim Basin, Basso *et al.* (2018) in the Campos Basin, and Aboaba and Liner (2020) in the Western Arkoma Basin. Similarly, Russel-Houston and Gray (2014) described the occurrence of paleokarst dissolutions in the form of sinkholes associated with faults, erosional truncations, and unconformities. Chaos and variance attributes reveal the chaotic nature of the sinkhole geometry (Ahlborn *et al.* 2014, Russel-Houston and Gray 2014). Image logs from W11 and W4 (Fig. 15) located within high amplitude

zones on the seismic (Fig. 9), corresponding to the Alagoas unconformity, confirm the occurrence of open and enlarged fractures as well as vuggy zones.

Hunt *et al.* (2010) described the occurrence of paleokarst features occurring as discontinuous amplitude anomalies arranged in separate subparallel reflection zones (Table 2), with a depth sag effect due to the collapse of the surrounding damaged rocks as seen in Fig. 14. This sag effect was initially reported by Purdy and Bertram (1993) and then by Story *et al.* (2000) as either linear or circular features caused by fracture corridor collapse.

Highly fractured/faulted regions (Fig. 13) may have resulted from overburden pressure above cave passages. The surrounding rocks get subjected to maximum tension and sagging, upon which the ceiling tends to collapse completely or partially. This process could be responsible for the development of damaged/fractured zones (Figs. 8, 11, and 12), which may connect several closely spaced karst features giving rise to high permeability. The permeability may be significantly reduced in cases where these regions are filled with fine materials or breccia transported by flowing fluids within the karst conduits or in cases where these Paleokarst passages get buried deeper and subjected to extensive mechanical compaction resulting in brecciated facies or overpressure zones from pressured solutions in these passages.

The absence of vertical pipe-like structure popularly attributed to sinkholes (Rodriguez *et al.* 2017, Aboaba and Liner 2020) and canyons (Basso *et al.* 2018) in the study area may be due to dissolutions close to the vadose zone resulting in laterally extending dissolutions rather than gravity influenced vertically extending dissolutions, with an exception for faults/fractures influenced karstifications that follow the paths of the discontinuities (Figs. 10 and 14).

The extensional tectonics during the sag phase supports the creation of reworked and fractured facies along brecciated zones that have been identified in this work using the borehole image logs (Fig. 15). These reworked facies could have also been sourced from the widespread weathering process that we believed to be associated with the unconformities as identified by Dorobek *et al.* (2012), Herlinger Jr. *et al.* (2017), and Basso *et al.* (2020); along the Barra Velha deposits, where some of them are located above the Intra-Alagoas unconformity (IAU) supporting the hypothesis of the intensive weathering events. Some literature described the occurrence of high porosity zones associated with dissolution at a widespread paleo-exposure surface resulting in an open pore network with abundant moldic and intercrystalline porosity, identified as various styles of karstification in the pre-salt succession from borehole image logs, including vuggies, open and enlarged faults, and caves (Jesus *et al.* 2019). These weathered and fractured zones identified in this work are related to the disrupted, discontinuous, and chaotic seismic reflections as described in Table 2. The conceptual model (Fig. 16) exemplifies the main occurrences of fractured and karstified zones inside the studied area. The structural high zones are more susceptible to diagenetic dissolution and karstification processes when compared with the structural low position.

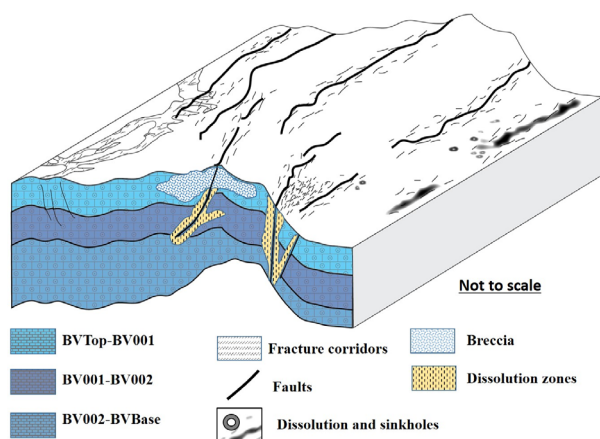


Figure 16. Model illustrating fracture-aided dissolution mechanism with structural control in the Barra Velha Formation in the studied pilot area. The fractures provide a pathway for the dissolution fluids to circulate and enlarge the existing fractures, which eventually leads to the formation of brecciated units and sinkholes in the formation. The overall control of the fracture-dissolution process is believed to be influenced by the existing structural framework of the area, which includes major faults, minor faults, and fractures that provide the necessary pathways for fluids.

Mechanism of carbonate dissolution

Faults and fractures/brecciation

The presence of anomalous bright spots associated with the fault and discontinuity networks suggests that these features are important conduits for fluid flow and dissolution and that they play a key role in the development of karst landscapes in the study area. The high density of fracture-aided karst features (Klimchouk *et al.* 2012) in the structural highs of the Barra Velha formation (Figs. 8, 9, 11, 12, 14, and 16) suggests that surface processes are the predominant agent in the karstification process. The dissolutions may coincide with the subaerial weathering process, which led to the deposition of reworked facies toward the top of the Barra Velha Formation. The occurrence of silicate injections from hydrothermal fluid alteration was reported in the basal section of the Barra Velha Formation (Lima and De Ros 2019), which also explains the presence of dissolutions and karst-related features. These subsurface dissolution processes are currently a subject of deliberation, especially since distinguishing between dissolutions made by surface-sourced charged water and those made by subsurface hydrothermal flow is very difficult without the use of core analysis and geochemical evaluations.

Movement of charged fluids in pores

Rauch and White (1977) showed that the minimum pore or fracture aperture of 25 μm can facilitate karst development. This is because, at this size, there is not only enough space for fluid to flow and dissolve the rock but also enough confinement to keep the water and dissolved minerals in contact with the rock surface for a longer period. Although there seems to be a mineralogical control over the dissolution rate, the greater the initial aperture (fissure or pore) the faster the propagation (extension) of the dissolution. In the Barra Velha Formation, facies rich in mud would have limited dissolution through this process as the pore spaces are clogged and there is minimal or no flow of fluids through the pores with exceptions along the fractures and faults. The spherulites and shrub facies with spherical to sub-spherical coarse grains are relatively porous (Basso *et al.* 2020) and, as such, may contribute a great deal to the dissolution process as they allow for free flow of charge fluids in the carbonates of the Barra Velha Formation.

CONCLUSION

Paleokarst systems associated with damaged zones were identified within the Aptian carbonates of the Barra Velha Formation in the Santos Basin using seismic attributes and well data analysis. Although the seismic resolution was limiting as direct Seismic-Image log integration was not feasible and only karst features greater than or equal to the resolution of the seismic could be analyzed, the image logs were helpful to enhance the knowledge and navigation of the karst pore scales and resolutions.

Open and closed fractures and vuggy and brecciated zones characterize the paleokarst system of this pilot area of the Santos Basin as evident from the seismic and borehole image log. The principal agents of karstification are likely an effect of dynamically charged fluids sourced from the surface or within the formation and circulating in the vadose zone, as well as from deep-seated hydrothermal events. Seismic attributes show a preferred trend of these karstified zones aligning to the brittle and fracture trends in the Northwest and Southeast directions. The intensity and absence of well-developed pipe structures and erosive canyon support the hypothesis of development through a cluster of fracture networks and depressions, which could have emerged due to diagenesis, tectonic uplifts, and subareal erosion.

Further analysis is required to improve the understanding of the spatial occurrence and distribution of these systems, especially when cores and extended seismic volumes become available. As core and production information becomes available, greater confidence as it relates to the interconnectivity of the karst systems and how they may affect production can be established.

ACKNOWLEDGMENTS

We gratefully acknowledge the support of EPIC—Energy Production Innovation Center, hosted by the Universidade Estadual de Campinas (UNICAMP) and sponsored by Equinor and FAPESP—São Paulo Research Foundation (2020/08919-7) through the EMUs Process. We also acknowledge the support of ANP (Brazil's National Oil, Natural Gas, and Biofuels Agency) through the R&D levy regulation, Emerson, and LMKR holdings for the software licenses and data used in this work. Acknowledgments are extended to the Center for Petroleum Studies (CEPETRO), the School of Mechanical Engineering (FEM), and the Geological Modelling and Reservoir Characterization (MGR) group.

ARTICLE INFORMATION

Manuscript ID: 20220073. Received on: 07 OCT 2022. Approved on: 05 MAR 2023.

How to cite this article: Nworie D.C., Chinelatto G.F., Vidal A.C. 2023. Paleokarst features in the aptian carbonates of the Barra Velha Formation, Santos Basin, Brazil. *Brazilian Journal of Geology*, 53(1):e20220073. <https://doi.org/10.1590/2317-4889202320220073>

D.C.N.: Conceptualization, Formal Analysis, Investigation, Methodology, Software, Validation, Visualization, Writing—original draft, and Writing—review & editing. G.F.C.: Data Curation, Formal Analysis, Investigation, Methodology, Project Administration, Software, Validation, Visualization, Writing—original draft, and Writing—review & editing. A.C.V.: Conceptualization, Funding Acquisition, Project Administration, Resources, Software, Supervision, Validation, and Writing—review & editing.

Competing interest: the authors declare no competing interests.

REFERENCES

- Aboaba O., Liner C. 2020. Interpretation of Paleozoic paleokarst features in the Arkoma Basin of Oklahoma using 3D seismic and well logs. Society of Exploration Geophysicists and the American Association of Petroleum Geologists. *Interpretation*, 8(2):T421-T440. <https://doi.org/10.1190/INT-2019-0155.1>
- Ahlborn M., Stemmerik L., Kalstø T.K. 2014. 3D seismic analysis of karstified interbedded carbonates and evaporites, Lower Permian Gipsdalen Group, Loppa High, southwestern Barents Sea. *Marine and Petroleum Geology*, 56:16-33, <https://doi.org/10.1016/j.marpetgeo.2014.02.015>
- Basso M., Belila A.M.P., Chinelatto G.F., Souza J.P.P., Vidal A.C. 2020. Sedimentology and petrophysical analysis of pre-salt lacustrine carbonate reservoir from the Santos Basin, southeast Brazil. *International Journal of Earth Sciences*, 110:2573-2595. <https://doi.org/10.1007/s00531-020-01932-7>
- Basso M., Kuroda M.C., Afonso L.C.S., Vidal A.C. 2018. Three-dimensional seismic geomorphology of paleokarst in the Cretaceous Macaé group carbonates, Campos Basin, Brazil. *Journal of Petroleum Geology*, 41(4):513-526. <https://doi.org/10.1111/jpg.12719>
- Beasley C.J., Fidak J.C., Bize E., Boyd E., Frydman M., Zerilli A., Dribus J.R., Moreira J.L., Pinto C.C.A. 2010. *Brazil's Presalt Play*. Oilfield Review Autumn, Schlumberger.
- Boersma Q., Prabhakaran R., Bezerra F.H., Bertotti G. 2019. Linking natural fractures to karst cave development: a case study combining drone imagery, a natural cave network and numerical modelling. *Petroleum Geoscience*, 25(4):454-469. <https://doi.org/10.1144/petgeo2018-151>
- Brown A.B. 2001. Understanding seismic attributes. *Geophysics*, 66(1):47-48. <https://doi.org/10.1190/1.1444919>
- Bruhn C.H.L., Pinto A.C.C., Johann P.R.S., Branco C.C.M., Salomão M.C., Ednilson B.F. 2017. Campos and Santos Basins: 40 Years of Reservoir Characterization and Management of Shallow- to Ultra-Deep Water, Post- and Pre-Salt Reservoirs - Historical Overview and Future Challenges. In: OTC Brasil, 2017, Rio de Janeiro. *Anais...* <https://doi.org/10.4043/28159-MS>
- Ceraldi S.T., Green D.R. 2016. Evolution of the South Atlantic lacustrine deposits in response to Early Cretaceous rifting, subsidence, and lake hydrology. *Special Publications*, 438:77-98. <https://doi.org/10.1144/SP438.10>
- Chinelatto G.F., Belia A.M.P., Basso M., Souza P.P.J., Vidal A.C. 2020. A taphofacies interpretation of shell concentrations and their relationship with petrophysics: A case study of Barremian-Aptian coquinas in the Itapema Formation, Santos Basin-Brazil. *Marine and Petroleum Geology*, 116(2020):104317. <https://doi.org/10.1016/j.marpetgeo.2020.104317>
- Chopra S., Marfurt K.J. 2007. *Seismic attributes for prospect identification and reservoir characterization*. Tulsa: Society of Exploration Geophysicists, European Association of Geoscientists & Engineers. (Geophysical development series; v. 11.)
- Chung E.K.Y., Ting K.K., Aljaaidi O. 2011. Karst modeling of a Miocene carbonate build-up in Central Luconia, SE Asia: Challenges in seismic characterization and geological model building. In: International Petroleum Technology Conference. *Anais...* OnePetro.
- Diabat A., Ahmad F., Hammouri N., Obeidat M.M. 2015. Karst development related to extensional fracture network at Bany-Kanana area, northern Jordan. *Arabian Journal of Geosciences*, 8:4999-5014. <https://doi.org/10.1007/s12517-014-1568-7>
- Dorobek S., Piccoli L., Coffey B., Adams A. 2012. Carbonate rock forming processes in the Pre-salt "Sag" successions of Campos Basin, Offshore Brazil: Evidence for seasonal dominantly abiogenic carbonate precipitation, substrate controls, and broader geologic implications. In: AAPG Hedberg Conference Microbial Carbonate Reservoir Characterization, 2012, Houston. *Abstracts...*
- Farias F.A., Sztamari P., Bahniuk A., França A.B. 2019. Evaporitic carbonates in the pre salt of Santos Basin – genesis and tectonic implications. *Marine and Petroleum Geology*, 105(2019):251-272. <https://doi.org/10.1016/j.marpetgeo.2019.04.020>
- Ford D., Williams P. 2007. *Karst hydrogeology and geomorphology*. New York: John Wiley and Sons.
- Gomes J.P., Bunevich R.B., Tedeschi L.R., Tucker M.E., Whitaker F.F. 2020. Facies classification and patterns of lacustrine carbonate deposition of the Barra Velha Formation, Santos Basin, Brazilian Pre-salt. *Marine and Petroleum Geology*, 113(2020):104176. <https://doi.org/10.1016/j.marpetgeo.2019.104176>
- Herlinger Jr. R., Zambonato E.E., De Ros L.F. 2017. Influence of diagenesis on the quality of Lower Cretaceous pre-salt lacustrine reservoirs from northern Campos Basin, offshore Brazil. *Journal of Sediment Research*, 87(12):1285-1313. <https://doi.org/10.2110/jsr.2017.70>
- Hunt D., Colpaert A., Miquelis F., Graham-Wall B., Pajchel J., Lukasiak J., Rafaelsen B., Avu A., Patton G. 2010. Seismic geomorphology of paleokarst systems in Paleozoic carbonates, Norwegian Barents Sea. In: Wood L. J., Simo T. T., Rosen N.C. (eds.). Proceedings of the 30th Annual GCSSEPM Foundation Bob F Perkins Research Conference, p. 191-210.
- Janson X., Fomel S. 2011. 3-D Forward Seismic Model of an Outcrop-Based Geocellular Model. In: Martinsen O.J., Pulham A.J., Haughton P.D., Sullivan M.D. (eds.), *Outcrops Revitalized: Tools, Techniques and Applications*. SEPM Society for Sedimentary Geology, p. 87-106.
- Jesus C., Azul M.O., Lupinacci W.M., Machado L. 2019. Multiattribute framework analysis for the identification of carbonate mounds in the Brazilian presalt zone. *Interpretation*, 7(2):T467-T476. <https://doi.org/10.1190/INT-2018-0004.1>
- Kacaroglu F. 1999. Review of Groundwater Pollution and Protection in Karst Areas. *Water, Air and Soil Pollution*, 113:337-356. <https://doi.org/10.1023/A:1005014532330>
- Klimchouk A.B. 2013. 6.34 Evolution of Intrastratal Karst and Caves in Gypsum. *Treatise on Geomorphology*, 6:438-450. <https://doi.org/10.1016/B978-0-12-374739-6.00123-8>
- Klimchouk A.B., Auler A.S., Bezerra F.H.R., Cazarin C.L., Balsamo F., Dublyansky Y. 2016. Hypogenic origin, geologic controls and functional organization of a giant cave system in Precambrian carbonates, Brazil. *Geomorphology*, 253:385-405. <https://doi.org/10.1016/j.geomorph.2015.11.002>
- Klimchouk A.B., Tymokhina E., Amelichev G. 2012. Speleogenetic effects of interaction between deeply derived fracture-conduit flow and intrastratal matrix flow in hypogene karst settings. *International Journal of Speleology*, 41(2):35-55. <https://doi.org/10.5038/1827-806X.41.2.4>
- Kumar R., Perumalla S., Verma S.K. 2012. Geomechanical Evaluation of Mud Losses and Wellbore Instability in Mumbai High North Field—Implications to Infill Drilling and Reservoir Development. In: SPE Oil and Gas India Conference and Exhibition, 2012, Mumbai. *Anais...*
- Laurent A., Averbuch O., Beccaletto L., Graveleau F., Lacquement F., Capar L., Marc S. 2021. 3-D structure of the Variscan thrust front in northern France: New insights from seismic reflection profiles. *Tectonics*, 40(7):e2020TC006642. <https://doi.org/10.1029/2020TC006642>
- Leite C.O.N., Silva C.M.A., Ros L.F. 2020. Depositional and diagenetic processes in the Pre-salt rift section of a Santos Basin area, SE Brazil. *Journal of Sedimentary Research*, 90(6):584-608. <https://doi.org/10.2110/jsr.2020.27>
- Li B., Zhou Y., Li S., Ye Y., Liu H. 2022. Injection-production optimization of fault-karst reservoir—considering high-speed non-Darcy effect. *Journal of Petroleum Exploration and Production Technology*, 12:1023-1036. <https://doi.org/10.1007/s13202-021-01363-3>
- Li Y., Zhang L., Wang D., Shi S., Cui X. 2016. Hydrocarbon detection for Ordovician carbonate reservoir using amplitude variation with offset and spectral decomposition: Interpretation, 4(3):SN11-SN30. <https://doi.org/10.1190/INT-2015-0135.1>
- Lima B.E.M., De Ros L.F. 2019. Deposition, diagenetic and hydrothermal processes in the Aptian Pre-Salt lacustrine carbonate reservoirs of the northern Campos Basin, offshore Brazil. *Sedimentary Geology*, 383:55-81. <https://doi.org/10.1016/j.sedgeo.2019.01.006>
- Liu Y., Wang Y. 2017. Seismic Characterization of a carbonate reservoir in Tarim Basin. *Geophysics*, 82(5):B177-B188. <https://doi.org/10.1190/geo2016-0517.1>

- Loucks R. 1999. Paleocave carbonate reservoirs: origins, burial-depth modifications, spatial complexity and reservoir implications. *AAPG Bulletin*, **83**(11):1795-1834. <https://doi.org/10.1306/E4FD426F-1732-11D7-8645000102C1865D>
- Mahry A., Suryadi D., Sufiadi E., Hadinata D., Wahyudi Y. 2016. Well Control in Carbonate Zone—Total Loss and Kick in Gas Reservoir. In: Offshore Technology Conference, 2016, Houston. *Anais...*
- Maksimov D., Pavlov A., Sangesland S. 2021. Prediction and Early Detection of Karsts—An overview of Methods and Technologies for safer Drilling in Carbonates. *Energies*, **14**(20):6517. <https://doi.org/10.3390/en14206517>
- Milad B., Slatt R. 2017. Integrated 3D seismic and core data for characterization of natural fractures of the Hunton Limestone and the Woodford Shale in Central Oklahoma. In: AAPG 2017 Annual Convention and Exhibition, 2017, Houston. *Anais...* <https://doi.org/10.13140/RG.2.2.24808.37121>
- Mizusaki A.M.P., Petrini R., Bellieni G., Comin-Chiaromonti P., Dias J., De Min A., Piccirillo E.M. 1992. Basalt magmatism along the passive continental margin of SE Brazil (Campos Basin). *Contributions to Mineralogy and Petrology*, **111**:143-160. <https://doi.org/10.1007/BF00348948>
- Moreira J.L.P., Madeira C.V.M., Gil J.A., Machado M.A.P. 2007. Bacia de Santos. *Boletim de Geociências da Petrobras*, **15**(2):531-549.
- Okubo J., Lykawka R., Warren L.V., Favoreto J., Dias-Brito D. 2015. Depositional, diagenetic and stratigraphic aspects of Macaé Group carbonates (Albian): example from an oilfield from Campos Basin. *Brazilian Journal of Geology*, **45**(2):243-258. <https://doi.org/10.1590/23174889201500020005>
- Oliveira V.C.B., Silva C.M.A., Borghi L.F., Carvalho I.S. 2019. Lacustrine coquinas and hybrid deposits from rift phase: pre-Salt, lower Cretaceous, Campos Basin, Brazil. *Journal of South American Earth Sciences*, **95**:102254. <https://doi.org/10.1016/j.jsames.2019.102254>
- Purdy E.G., Bertram G.T. 1993. Carbonate concepts from the Maldives, Indian Ocean. *AAPG Studies in Geology*, **34**:7-55. <https://doi.org/10.1306/St34568>
- Purdy E.G., Waltham D. 1999. Reservoir implications of modern karst topography. *AAPG Bulletin*, **83**(11):1774-1793. <https://doi.org/10.1306/E4FD4265-1732-11D7-8645000102C1865D>
- Qi J., Zhang B., Zhou H., Marfurt K. 2014. Attribute expression of fault-controlled karst — Fort Worth Basin, Texas: A tutorial. *Interpretation*, **2**(3):SF91-SF110. <https://doi.org/10.1190/INT-2013-0188.1>
- Radovich B.J., Oliveros R.B. 1998. 3-D sequence interpretation of seismic instantaneous attributes from the Gorgon field. *The Leading Edge*, **17**(9):1286-1293.
- Rauch H.W., White W.B. 1977. Dissolution kinetics of carbonate rocks, 1. Effects of lithology on dissolution rate. *Water Resources Research*, **13**(2):381-394. <https://doi.org/10.1029/WR013i002p00381>
- Ribeiro da Silva S.F., Pereira E. 2017. Tectono-stratigraphic evolution of Lapa field pre-salt section, Santos Basin (SE Brazilian continental margin). *Journal of Sedimentary Environments*, **2**(2):133-148. <https://doi.org/10.12957/jse.2017.30052>
- Roberts A. 2001. Curvature attributes and their application to 3D interpreted horizons. *First Break*, **19**(2):85-100. <https://doi.org/10.1046/j.0263-5046.2001.00142.x>
- Rodriguez C.R., Jackson C.A.-L., Bell R.E., Rotevatn A., Francis M. 2017. *Submarine salt dissolution in the Santos Basin, offshore Brazil*. London: Basins Research Group (BRG), Department of Earth Science & Engineering, Imperial College, SW7 2BP.
- Russel-Houston J., Gray K. 2014. Paleokarst in the Grosmont Formation and reservoir implications, Saleski, Alberta, Canada. *Interpretation*, **2**(3):SF29-SF50. <https://doi.org/10.1190/int-2013-0187.1>
- Sallee A., Dick H., Sudhakar V., Morgan A., Payton S., Paddock D. 2019. Managing Drilling Losses in the Permian Using Airborne Gravity Full Tensor Gradiometry. In: SPE/IADC International Drilling Conference and Exhibition, 2019, The Hague. *Anais...*
- Shelf R.E. 2002. *Encyclopedic Dictionary of Applied Geophysics*. 4^a ed. SEG.
- Story C., Peng P., Heubeck C., Sullivan C., Lin J.D. 2000. Liuhua 11-1 Field, South China Sea: A shallow carbonate reservoir developed using ultrahigh-resolution 3-D seismic, inversion, and attribute-based reservoir modeling. *The Leading Edge*, **19**(8):834-844. <https://doi.org/10.1190/1.1438721>
- Sullivan C.E., Marfurt K.J., Lacazette A., Ammerman M. 2006. Application of new seismic attributes to collapse chimneys in the Fort Worth Basin. *Geophysics*, **71**(4):B111-B119. <https://doi.org/10.1190/1.2216189>
- Sun Q., Cartwright J., Wu S., Chen D. 2013. 3D seismic interpretation of dissolution pipes in the South China Sea: Genesis by subsurface, fluid induced collapse. *Marine Geology*, **337**:171-181. <https://doi.org/10.1016/j.margeo.2013.03.002>
- Sun S.Z., Liu L.F., Du T. 2016. Karst carbonate reservoir identification using frequency dependent AVO inversion in Tarim Basin, China. In: Conference and Exhibition, 78., 2016. *Extended Abstracts...*
- Tanaka A.P.B., Borges J.G.P., Matos G.C., Campos M.T.R., Cunha M.B., Souza R.B., Caldeira J.N.M., Oliveira T.A.S., Marçon D.R., Lima A.P.M. 2022. Fault-related fracture modeling in a pre-salt lacustrine carbonate reservoir from Santos Basin, offshore Brazil: Predicting preferential fluid flow paths using 3D geological and flow simulation models. *Marine and Petroleum Geology*, **135**:105392. <https://doi.org/10.1016/j.marpetgeo.2021.105392>
- Tang Y., Yunfeng Z., Hongming T., Zhenyu W., Jianxin Z., Xiaochen Y., Liang X. 2021. Carbonate burial dissolution related to faults and fractures in the Triassic Daye Formation of the Huandiqiao Section, Huangshi Area, Hubei, China. *Canadian Journal of Earth Sciences*, **58**(1):38-49. <https://doi.org/10.1139/cjes-2019-0177>
- Tian F., Jin Q., Lu X., Lei Y., Zhang L., Zheng S., Zhang H., Rong Y., Liu N. 2016. Multi-layered Ordovician paleokarst reservoir detection and spatial delineation: A case study in the Tahe Oilfield, Tarim Basin, Western China. *Marine and Petroleum Geology*, **69**:53-73. <https://doi.org/10.1016/j.marpetgeo.2015.10.015>
- Trice R. 2005. Challenges and insights in optimizing oil production from Middle East mega karst reservoirs. In: SPE Middle East Oil and Gas Show and Conference, Kingdom of Bahrain, 2005. *Anais...* <https://doi.org/10.2118/93679-MS>
- Vahrenkamp V.C., David F., Duijndam P., Newall M., Crevello P. 2004. Growth architecture, faulting, and karstification of a middle Miocene carbonate platform, Luconia Province, offshore Sarawak, Malaysia. *AAPG Memoir*, **81**:329-350.
- Vincentelli M.G.C., Favoreto J., Oliveira R.E. 2017. Paleogeographic evolution of carbonate reservoirs: geological and geophysical analysis at the Albian Campos Basin, Brazil. *Journal of Geophysics Engineering*, **15**(1):26-41. <https://doi.org/10.1088/1742-2140/aa83ca>
- Wang J., Zhao L., Zhang X., Yang Z., Cao H., Chen L., Shan F., Liu M. 2015. *Buried hill karst reservoirs and their controls on productivity*. Research Institute of Petroleum Exploration and Development, PetroChina.
- Watkins H., Healy D., Bond C.E., Butler R.W.H. 2018. Implications of heterogeneous fracture distribution on reservoir quality; an analogue from the Torridon Group sandstone, Moine Thrust Belt, NW Scotland. *Journal of Structural Geology*, **108**:180-197. <https://doi.org/10.1016/j.jsg.2017.06.002>
- Wright V.P., Barnett A.J. 2015. An abiotic model for the development of textures in some South Atlantic early Cretaceous lacustrine carbonates. *Special Publications*, **418**:209-219. <https://doi.org/10.1144/SP418.3>
- Wright V.P., Barnett A.J. 2017a. Classifying Reservoir Carbonates When the Status Quo Simply Does Not Work: A Case Study from the Cretaceous of the South Atlantic. In: AAPG Search and Discovery. *Anais...*
- Wright V.P., Barnett A.J. 2017b. Critically Evaluating the Current Depositional Models for the Pre-Salt Barra Velha Formation, Offshore Brazil. In: AAPG Search and Discovery. *Anais...*
- Wright V.P., Smart P.L. 1994. Paleokarst (Dissolution Diagenesis): its Occurrence and Hydrocarbon Exploration Significance. Diagenesis, IV. *Developments in Sedimentology*, **51**:477-517. [https://doi.org/10.1016/S0070-4571\(08\)70447-3](https://doi.org/10.1016/S0070-4571(08)70447-3)
- Xiaoxia Z., Jiajie Y., Nianyin L., Chao W. 2021. Multi-scale fracture prediction and characterization method of a fractured carbonate reservoir. *Journal of Petroleum Exploration and Production*, **11**:191-202 <https://doi.org/10.1007/s13202-020-01033-w>
- Xu C., Di B., Wei J. 2016. A physical modeling study of seismic features of karst cave reservoirs in the Tarim Basin, China. *Geophysics*, **81**(1):B31-B41. <https://doi.org/10.1190/geo2014-0548.1>

- Yao Y., Sa L., Wang S. 2005. Research on the seismic wave field of karst cavern reservoirs near deep carbonate weathered crusts. *Applied Geophysics*, **2**:94-102. <https://doi.org/10.1007/s11770-005-0040-6>
- Yu J., Li Z., Yang L. 2016. Fault system impact on paleokarst distribution in the Ordovician Yingshan Formation in the central Tarim basin, northwest China. *Marine and Petroleum Geology*, **71**:105-118. <https://doi.org/10.1016/j.marpetgeo.2015.12.016>
- Zeng H., Wang G., Janson X., Loucks R., Xia Y., Xu L., Yuan B. 2011. Characterizing seismic bright spots in deeply buried, Ordovician Paleokarst strata, Central Tabei uplift, Tarim Basin, Western China. *Geophysics*, **76**(4):B127-B137. <https://doi.org/10.1190/1.3581199>
- Zeng H., Wang Q., Loucks B., Janson X., Xia Y., Xu L. 2010. Seismic geomorphologic, core, and outcrop expression of an Ordovician paleokarst system in north-central Tarim Basin, China. In: Wood L.J., Simo T.T., Rosen N.C., eds. *Seismic imaging of depositional and geomorphologic systems*: 30th Annual GCSSEPM Foundation Bob F. Perkins Research Conference, CD-ROM, p. 73-87.
- Zhang W., Duan T., Li M., Zhao H., Shang X., Wang Y. 2021. Architecture characterization of Ordovician fault-controlled paleokarst carbonate reservoirs in Tuoputai, Tahe oilfield, Tarim Basin, NW China. *Petroleum Exploration and Development*, **48**(2):367-380. [https://doi.org/10.1016/S1876-3804\(21\)60029-0](https://doi.org/10.1016/S1876-3804(21)60029-0)